

High efficiency plasmonic probe design for parallel near-field optics applications

Guanghao Rui,^{1,2} Weibin Chen,¹ and Qiwen Zhan^{1*}

¹*Electro-Optics Graduate Program, University of Dayton, 300 College Park, Dayton Ohio 45469, USA*

²*Department of Optics and Optical Engineering, University of Science and Technology of China, Hefei, Anhui 230026, China*

*qiwen.zhan@notes.udayton.edu

Abstract: We study a high efficiency plasmonic near-field probe that integrates a spiral plasmonic lens and a sharp conical tip under circular polarized illumination. To achieve high field enhancement, two layers of spiral plasmonic lens and a composite tip design are adopted. The plasmonic probe exhibits optical spin dependence due to the use of spiral plasmonic lens. Under 633 nm wavelength excitation, an electric field enhancement factor of 366 and circular polarization extinction ratio of 81 can be achieved. Such a spin dependence enables the hot spot at the tip apex to be switched on and off by modulating the polarization handedness. The probe can be made in an array format that is suitable for large area parallel near-field optics applications such as lithography and microscopy.

©2011 Optical Society of America

OCIS codes: (230.5440) Polarization-selective devices; (240.6680) Surface plasmons; (260.5430) Polarization; (260.6042) Singular optics; (180.5810) Scanning microscopy; (110.4235) Nanolithography.

References and links

1. F. M. Schellenberg, "Resolution enhancement technology: the past, the present, and extensions for the future," in *Optical Microlithography XVII*, B. W. Smith, ed., Proc. SPIE **5377**, 1–20 (2004).
2. J. P. Silverman, "Challenges and progress in x-ray lithography," *J. Vac. Sci. Technol. B* **16**(6), 3137–3141 (1998).
3. L. P. Ghislain, V. B. Elings, K. B. Crozier, S. R. Manalis, S. C. Minne, K. Wilder, G. S. Kino, and C. F. Quate, "Near-field photolithography with a solid immersion lens," *Appl. Phys. Lett.* **74**(4), 501–503 (1999).
4. J. K. Chua, V. M. Murukeshan, S. K. Tan, and Q. Y. Lin, "Four beams evanescent waves interference lithography for patterning of two dimensional features," *Opt. Express* **15**(6), 3437–3451 (2007).
5. V. M. Murukeshan, J. K. Chua, S. K. Tan, and Q. Y. Lin, "Nano-scale three dimensional surface relief features using single exposure counterpropagating multiple evanescent waves interference phenomenon," *Opt. Express* **16**(18), 13857–13870 (2008).
6. W. L. Barnes, A. Dereux, and T. W. Ebbesen, "Surface plasmon subwavelength optics," *Nature* **424**(6950), 824–830 (2003).
7. X. Guo, J. Du, Y. Guo, and J. Yao, "Large-area surface-plasmon polariton interference lithography," *Opt. Lett.* **31**(17), 2613–2615 (2006).
8. M. He, Z. Zhang, S. Shi, J. Du, X. Li, S. Li, and W. Ma, "A practical nanofabrication method: surface plasmon polaritons interference lithography based on backside-exposure technique," *Opt. Express* **18**(15), 15975–15980 (2010).
9. X. Luo, and T. Ishihara, "Surface plasmon resonant interference nanolithography technique," *Appl. Phys. Lett.* **84**, 4780–4782 (2004).
10. L. Wang, E. X. Jin, S. M. Uppuluri, and X. Xu, "Contact optical nanolithography using nanoscale C-shaped apertures," *Opt. Express* **14**(21), 9902–9908 (2006).
11. R. Guo, E. C. Kinzel, Y. Li, S. M. Uppuluri, A. Raman, and X. Xu, "Three-dimensional mapping of optical near field of a nanoscale bowtie antenna," *Opt. Express* **18**(5), 4961–4971 (2010).
12. S. M. Uppuluri, E. C. Kinzel, Y. Li, and X. Xu, "Parallel optical nanolithography using nanoscale bowtie aperture array," *Opt. Express* **18**(7), 7369–7375 (2010).
13. W. Chen, D. C. Abeysinghe, R. L. Nelson, and Q. Zhan, "Plasmonic lens made of multiple concentric metallic rings under radially polarized illumination," *Nano Lett.* **9**(12), 4320–4325 (2009).
14. G. M. Lerman, A. Yanai, and U. Levy, "Demonstration of nanofocusing by the use of plasmonic lens illuminated with radially polarized light," *Nano Lett.* **9**(5), 2139–2143 (2009).
15. Q. Zhan, "Evanescent Bessel beam generation via surface plasmon resonance excitation by a radially polarized beam," *Opt. Lett.* **31**(11), 1726–1728 (2006).

16. W. Chen, and Q. Zhan, "Realization of an evanescent Bessel beam via surface plasmon interference excited by a radially polarized beam," *Opt. Lett.* **34**(6), 722–724 (2009).
17. G. Rui, W. Chen, Y. Lu, P. Wang, H. Ming, and Q. Zhan, "Plasmonic near-field probe using the combination of concentric rings and conical tip under radial polarization illumination," *J. Opt.* **12**(3), 035004–035009 (2010).
18. A. Normatov, P. Ginzburg, N. Berkovitch, G. M. Lerman, A. Yanai, U. Levy, and M. Orenstein, "Efficient coupling and field enhancement for the nano-scale: plasmonic needle," *Opt. Express* **18**(13), 14079–14086 (2010).
19. P. Ginzburg, A. Nevet, N. Berkovitch, A. Normatov, G. M. Lerman, A. Yanai, U. Levy, and M. Orenstein, "Plasmonic resonance effects for tandem receiving-transmitting nanoantennas," *Nano Lett.* **11**(1), 220–224 (2010).
20. S. Yang, W. Chen, R. L. Nelson, and Q. Zhan, "Miniature circular polarization analyzer with spiral plasmonic lens," *Opt. Lett.* **34**(20), 3047–3049 (2009).
21. Z. Wu, W. Chen, D. C. Abeysinghe, R. L. Nelson, and Q. Zhan, "Two-photon fluorescence characterization of spiral plasmonic lenses as circular polarization analyzers," *Opt. Lett.* **35**(11), 1755–1757 (2010).
22. W. Chen, D. C. Abeysinghe, R. L. Nelson, and Q. Zhan, "Experimental confirmation of miniature spiral plasmonic lens as a circular polarization analyzer," *Nano Lett.* **10**(6), 2075–2079 (2010).
23. T. Søndergaard, S. I. Bozhevolnyi, S. M. Novikov, J. Beermann, E. Devaux, and T. W. Ebbesen, "Extraordinary optical transmission enhanced by nanofocusing," *Nano Lett.* **10**(8), 3123–3128 (2010).
24. X. W. Chen, V. Sandoghdar, and M. Agio, "Highly efficient interfacing of guided plasmons and photons in nanowires," *Nano Lett.* **9**(11), 3756–3761 (2009).
25. E. U. Haq, Z. Liu, Y. Zhang, S. A. A. Ahmad, L. S. Wong, S. P. Armes, J. K. Hobbs, G. J. Leggett, J. Micklefield, C. J. Roberts, and J. M. R. Weaver, "Parallel scanning near-field photolithography: the snomipede," *Nano Lett.* **10**(11), 4375–4380 (2010).

1. Introduction

Photolithography has been the most widely used patterning technique in semiconductor manufacturing and micro-fabrication because of its excellent repeatability, high yield, low cost, and suitability for large-area fabrication. To keep up with the Moore's law and fabricate even smaller nanoscale feature sizes, photolithographic techniques using shorter working wavelength such as extreme ultraviolet light (EUV) and soft X-rays [1, 2] have been pushed forward. However, the complexity and cost for the instrument increase dramatically with decreasing exposure wavelengths. Alternative technical approaches have been developed to meet the challenges. For example, contact evanescent wave interference lithography (EIL) was proposed for large-area nanostructure lithography [3–5]. However, this technique has limitations such as short transmission distance, shallow exposure depth and low contrast that cause low efficiency and control difficulties in practice. Recently there are significant interests of plasmonic photolithography. Surface plasmons (SPs) are electromagnetic surface waves at the dielectric/metal interface formed through metal-photon interactions. Its shorter effective wavelength and the associated field enhancement [6] offer attractive features for the development of next generation photolithographic techniques. Several methods, including maskless surface plasmon polaritons interference lithography (SPPIL) [7], backside-exposure SPPIL [8], and surface plasmon resonant interference nanolithography technology (SPRINT) [9], have successfully demonstrated the feasibilities of using SPs in photolithography. However, these interferometric plasmonic lithography techniques are limited to periodic structures comprised of straight interference fringes and not suitable for the fabrication of complex patterns.

Other than the parallel patterning techniques, photolithographic techniques using near-field plasmonic probe have also been investigated. Plasmonic probes using c-shape ridge [10] and bowtie antennas [11] have been demonstrated for optical resolution better than the far field diffraction limit with enhanced light transmission. Nanoscale lithography with feature size of 85–90 nm has been realized [12] and complex patterns can be fabricated through point-by-point scanning in principle. However, the use of an aperture in these plasmonic probes limits the light throughput, consequently restricting the ultimate achievable line width. This problem can be solved by apertureless plasmonic probe lithography for which the resolution relies on the tip size and the local field intensity at the apex of the tip. In order to get higher near-field enhancement, SPs needs to be excited more efficiently. It has been demonstrated that optimal SPs excitation can be achieved through matching the axially symmetric structure to the polarization symmetry of radially polarized illumination [13–16], where the entire beam

is TM polarized with respect to the interface, enabling the SPs excitation from all directions and homogeneous focusing through constructive interference of these plasmon waves. Based on this observation, a new type of plasmonic near-field probe with high field enhancement that can be used in nanolithography has been proposed and studied. The probe integrates a sharp metallic conical tip at the center of a multiple concentric ring plasmonic lens [17–19]. Under radially polarized illumination, SPs can be efficiently excited and focused by the plasmonic lens and get further localized and enhanced by the metallic tip. Although this type of probe offers extremely high field enhancement, the singularity center of the radially polarized beam needs to be aligned to the center of the plasmonic lens structure. This necessitates a scanning mechanism that leads to slow writing speed and limit the realistic size of lithography area.

In this paper, we propose, optimize, and numerically analyze a novel near-field probe design that consists of a spiral plasmonic lens and a sharp conical tip at the center. Owing to the geometric phase effect, a spiral plasmonic lens focuses the circular polarization with an opposite chirality into a spot in the center, while defocusing the circular polarization with the same chirality into a donut shape. For a spiral with specific handedness, spatially separated plasmonic fields can be generated by switching the illuminated polarization between left-hand and right-hand circular (LHC and RHC) polarization, which has been demonstrated both by theory [20] and experiments [21, 22]. The tip at the center further collects the generated plasmonic wave and provides a highly enhanced local field at the tip end. Due to the different distributions of the plasmonic field generated by the spiral lens under LHC and RHC illuminations, the field intensity at the tip apex changes dramatically for different circular polarization illumination. More importantly, this probe design does not require a center alignment. Thus, it can be made in an array format where each probe can be readily switched on and off by changing the illumination polarization handedness. Such a dynamically reconfigurable nature along with the high efficiency of individual probe makes this design suitable for large area photolithography of complex patterns.

2. Individual composite probe design

The proposed probe structure is illustrated in Fig. 1. A 200 nm gold film is deposited onto a glass substrate. Two layers of left-handed single Archimedes's spiral slots with different slot width are etched into the gold film. In the cylindrical coordinates, a left-handed spiral (LHS) can be described as [20]

$$r = r_0 - \frac{\Lambda}{2\pi} \varphi, \quad (1)$$

where r_0 is a constant. The index of refraction for gold is $0.197+3.0908i$ at the 633 nm illumination wavelength, and the calculated SPs wavelength λ_{spp} is 598.8 nm. The parameters of the spiral described in Eq. 1 are $r_0=2\lambda_{spp}$ and $\Lambda=\lambda_{spp}$. The upper layer spiral (with slit width of 200 nm and height of 45 nm) is directly placed above the lower layer spiral (with slit width of 400 nm and height of 105 nm) with the same mid-point. A conical composite probe composed with a dielectric base and a sharp gold tip is placed in the center of spiral. The sharp conical shaped gold tip (with half-cone angle of 20° , base radius of 50 nm and apex radius of curvature of 10 nm) is located above a cylindrical glass base (with radius of 50 nm and height of 100 nm) as Fig. 1(c) shows. To reduce the reflection at the corner, the edge of the dielectric base is rounded with radius of 50 nm. Circularly polarized beam is used to illuminate the structure from the glass side at normal incidence.

A successful plasmonic near-field probe design should provide high coupling efficiency from the illumination to the desired near field hot spot while prevent far field radiation as much as possible. To increase the collection and coupling of the incident beam, spiral structure with multiple turns and wide slit width can be applied. However, the far field radiation loss will be high for wider slot opening. We adopt a two-layer spiral plasmonic lens structure shown in Fig. 1(b) to solve this dilemma. SPs are excited at the slot edge of the

lower spiral with wide opening to enlarge the SPs collection area while the upper spiral maintains narrow slot width to reduce the far field radiation. This approach is similar to the nanofocusing effect provided by V-groove structure reported recently [23]. Multiple turns are also used for both spiral plasmonic lenses to obtain better collection efficiency (shown in Fig. 1b). To provide structural support for the upper spiral, the slot of the lower spiral is filled with silicon dioxide. Both the slit width and height of each spiral plasmonic lens are optimized for maximal field enhancement. Compared with the previous one layer spiral design, this double layer spiral contributes to a higher field enhancement but maintains relative low radiation loss.

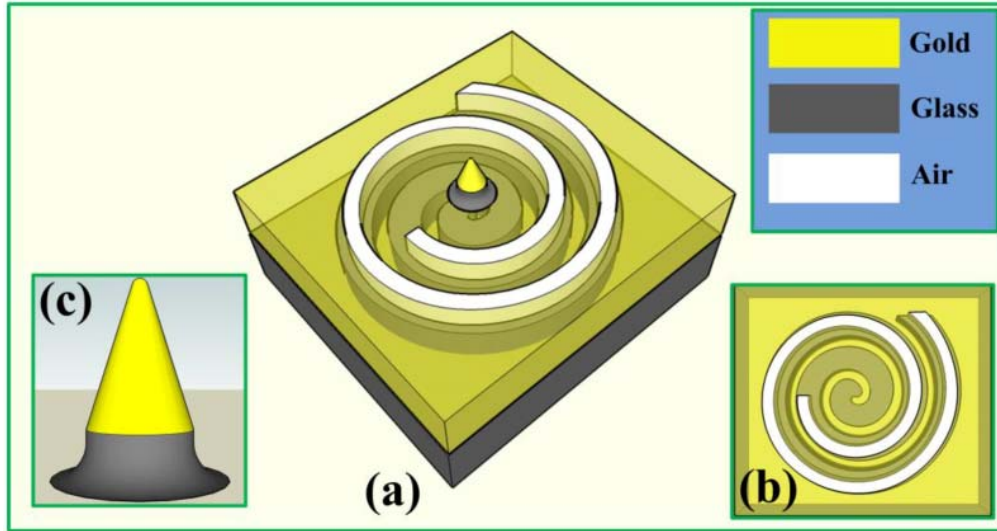


Fig. 1. (a) Diagram of plasmonic near-field probe that intergrates spiral plasmonic lens and a conical tip under circularly polarized illumination. Two layers of single Archimedes's spiral slots with different width and height are etched through gold film as a spiral plasmonic lens. A sharp composite tip is fabricated at the center of the spiral plasmonic lens structure. (b) The top view of the spiral plasmonic lens. (c) Schematic diagram of tip that combines a dielectric base and a metallic tip.

The SPs waves generated by the spiral plasmonic lens propagate along the gold/air surface and interfere with each other as they propagate towards the center. The plasmonic field distribution in the center relies on the handedness of incident circular polarization. It has been shown that RHC beam will be focused into a solid spot by a LHS structure, while the field distribution of LHC beam focused by a LHS structure is a doughnut with a dark center. Similarly, right-handed spiral (RHS) structure can focus RHC illumination into a doughnut spot, while into a homogeneous spot by LHC polarized illumination. This phenomenon can be explained from the coupling between the spin of incident photon and the chirality of the spiral lens. The topological charge of the plasmonic field in the center of the spiral is $l=(\sigma_s+\sigma_i)$, where the chirality of spiral is defined as $\sigma_s=+1$ for RHS and $\sigma_s=-1$ for LHS, the spins of the incident beam $\sigma_i=+1$ stands for RHC and $\sigma_i=-1$ stands for LHC similarly. Therefore a solid spot is generated for $l=0$ and doughnut spot for $l=\pm 2$ [22]. The tip in the center of the spiral lens further localizes the SPs and produce high field enhancement at the tip apex.

To obtain high field enhancement, a composite dielectric/metal tip is designed as opposed to a full metallic one. The dielectric base of the composite tip is used to improve the coupling between the plasmonic focal field produced by the spiral plasmonic lens into the conical metal tip above it. The glass base here can be regarded as an optical nano-fiber, and the coupling efficiency depends on the matching between the plasmonic surface mode and the guided mode of the nano-fiber. Figure 2(a) shows the distribution of the radial component E_r of the TEM_{01} mode for the fiber with a 50 nm radius glass core that is computed using the mode

analysis module of COMSOL. The plots of the radial component of the electrical field produced by the LHS structure illuminated by RHC and LHC polarization are shown respectively in Fig. 2(b) and 2(c). Please note that if the total intensity is plotted instead, a solid focal spot will appear for the case in Fig. 2(b) and a donut distribution will be resulted for the case in Fig. 2(c) due to the coupling between the spin of incident photon and the chirality of the spiral lens discussed above [20–22]. Figure 2(d) shows the linescan of the transverse electric field of above three plots. The solid blue curve is the theoretical transverse component of the electric field of TEM_{01} mode of the nano-fiber. The red broken line and black dot dash line show the transverse electric field of focused and defocused SPs waves in the vicinity of the spiral center. Clearly, the best overlapping between the surface modes and the TEM_{01} mode occurs for the electric field produced by the RHC illumination. The asymmetry of the surface modes are induced by the nonsymmetrical spiral plasmonic lens and the propagation loss of SPs, leading to the non-zero point in the middle of the surface modes. The guided photons propagate upwards in the dielectric base and couple to the metallic tip. The SPs waves converted from the guided photons of the dielectric base propagate along the surface of the metallic tip and get slowed down then adiabatically stopped at the tip apex, leading strongly enhanced local field at the tip apex. The height of the dielectric base is optimized to achieve the maximum field enhancement at the tip apex. Sufficiently small tip can be regard as an oscillating dipole that is driven by the SP waves and the large field enhancement is produced at the tip apex in a manner similar to the lightning rod effect. The coupling process describe above is similar to butt-coupling [24]. The radius of metallic tip is chosen to be the same as the dielectric base. The conversion efficiency between the dielectric base and metallic tip, which is defined as the ratio of the integration of the z component of the Poynting vector over two circular areas that are a few nanometres above and below the dielectric/gold interface of the probe, is about 85%. For smaller radius of the metallic tip, the conversion efficiency will decrease due to the larger radiation loss near the corner of the metallic tip.

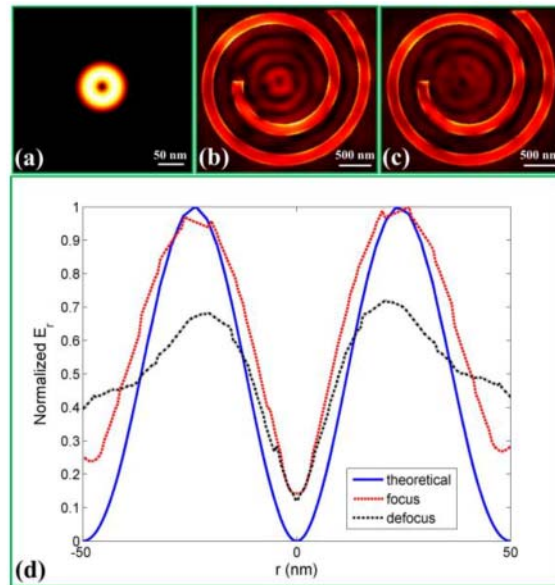


Fig. 2. (a) Transverse electric field distribution of the TEM_{01} mode for the fiber with a glass core and radius of 50 nm. Transverse electric field distribution of (b) LHS and (c) RHS structure without the sharp tip illuminated by RHC polarization. The color scaling in (b) and (c) are the same. (d) The linescan of the normalized (a), (b), and (c).

3. Three-dimensional finite element method modelling

A full 3D finite element method model (COMSOL) is developed to numerically investigate the characteristics of the entire structure. As we discussed before, the excited SPs propagate along the surface towards the center and further concentrate at the end of the tip, leading to a strong localized field. Because the field distribution depends on the handedness of the incident circularly polarized beam, the field intensity near the tip apex will change dramatically if we switch the polarization of the illumination between RHC and LHC. The electric field enhancement factor is defined as the peak electric field at the tip apex over the incident electric field of the circularly polarized illumination. Simulation results for LHS structure illuminated by RHC and LHC polarizations are shown in Fig. 3. For the LHS structure illuminated by RHC polarization (shown in Fig. 3(a)), the electric field enhancement factor is about 366. Figure 3(b) shows the same LHS structure under LHC polarized illumination instead. Owing to the donut distribution of the defocused field generated by the spiral plasmonic lens, the tip in the center cannot collect as much energy as that of the focused case and the electric field enhancement is only around 40.7. Identical color scaling is used for both Fig. 3(a) and 3(b) and clear contrast of the brightness at the tip apex can be observed. The circular polarization extinction ratio, which is defined as the ratio of the square of electric field enhancement factor between LHC and RHC polarized illuminations, is 81 for this probe.

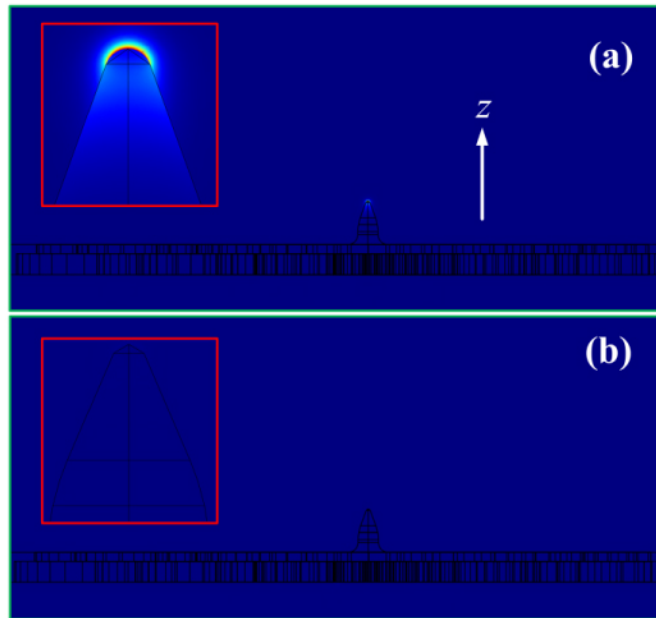


Fig. 3. Finite element method simulation results of the intensity distributions on the near-field probe with (a) LHS and (b) RHS under the same RHC polarized illumination. The color scaling is chosen to be identical for both plots to illustrate to contrast.

4. Effects of taper angle on field enhancement and extinction ratio

We also numerically calculated the electric field enhancement factor and extinction ratio for different half-cone angles of the conical tip while keeping the other parameters unchanged. The simulation results are summarized in Fig. 4. Figure 4(a) shows the electric field enhancement factor versus different half-cone angles. The maximal electric field enhancement is 366 at 20° and field enhancement factor higher than 300 can be maintained for half-cone angle between 18° - 23° . From 18° to 24° half-cone angles, extinction ratio higher than 80 can be maintained (Fig. 4(b)). Thus the performance of the tip does not strongly depend on the tip

cone angle. The less stringent requirement on the conical tip angle makes the fabrication much easier.

For comparison, we also investigated the case where the composite probe is replaced with a full metallic probe. We keep all the parameters of the structure the same except changing the material of the dielectric base to gold. As expected, the electric enhancement factor is much lower due to the higher reflection loss at the corner of the metallic base as well as the propagation loss along the metallic tip (Fig. 5(a)). The maximal electric field enhancement factor is 155 at a half-cone angle of 18°, which is much lower than the composite probe design. In addition, the electric enhancement factor quickly decreases as the half cone angle deviates from the optimal design value, requiring more strict control for the probe fabrication process. Figure 5(b) shows the dependence of the extinction ratio on the half-cone angle for the full metallic probe. Compared with Fig. 4(b), the extinction ratio for the full metallic probe is higher due to its much lower collection efficiency when the spiral plasmonic lens defocuses the illumination into a doughnut. In practical applications such as photolithography and imaging, manufacturability of the probe and larger field enhancement are much more important. Extinction ratio higher than 50 in general is enough to provide good contrast. Thus the composite probe is more advantageous over a full metallic tip design.

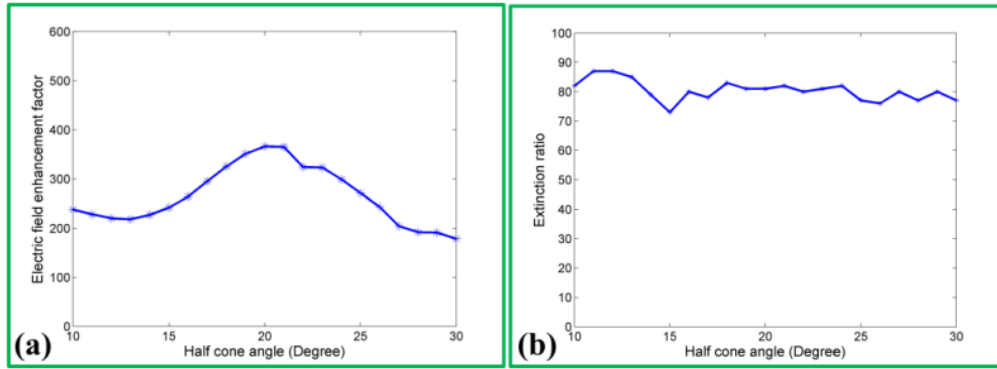


Fig. 4. (a) Electric field enhancement and (b) extinction ratio versus the half-cone taper angle of the tip for the probe comprises of a dielectric base and a metallic tip.

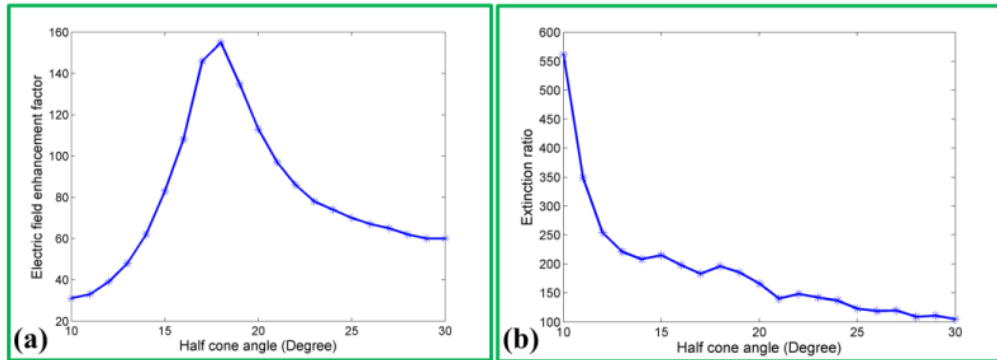


Fig. 5. (a) Electric field enhancement factor and (b) extinction ratio versus the half-cone taper angle of the tip for a full metallic probe.

4. Design and simulation of a probe array

One key advantage of the probe design is the elimination of the requirement of alignment between a singularity center of an illumination and a plasmonic lens structure, enabling its application in parallel near field processing with an array format [21, 25]. Figure 6(a) is the

scheme of 3×3 array that contains both LHS and RHS elements with the LHS elements forming a pattern of the letter “N”. The period of the array is $4 \mu\text{m}$, and the probe structure adopts the optimal parameters as shown in Fig. 3. Under RHC polarized illumination, those LHS elements corresponding to the letter “N” pattern will produce hot spots. Figure 6(b) is the simulated electric field at 10 nm above the tip end and clearly shows that the letter “N” formed by the LHS elements is lit up when illuminated by RCH polarization.

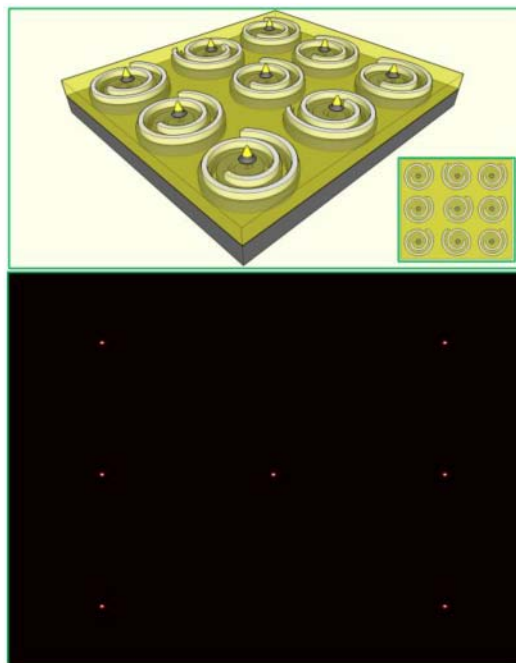


Fig. 6. (a) Scheme of the two dimensional array of the near-field probe. The spiral plasmonic lenses are either left-handed or right-handed. Top view is shown in the inset. (b) Simulated result of the intensity at 10 nm above the tip apex for RHC polarized illumination.

5. Conclusions

In conclusion, we designed and numerically studied a novel near-field probe design that combines a spiral plasmonic lens and a sharp conical tip. Double-layer Archimedes’s spiral plasmonic lens and a composite tip design are exploited to improve the coupling efficiency and optimize the field enhancement at the tip apex. The dielectric base of the composite tip couples focused plasmonic field efficiently, which can be explained by the good overlapping between the guided TEM_{01} mode of the dielectric base and the surface plasmon focus produced by the spiral plasmonic lens. Electric field enhancement factor of 366 can be achieved with 633 nm optical excitation wavelength. The probe design has a circular polarization extinction ratio higher than 80. The electric field enhancement factor and extinction ratio of this probe design do not strongly depend on the half-cone angle of the tip, allowing easier fabrication. Fabrication of the proposed probe is within the capabilities of modern nanofabrication tools. For example, focused ion beam milling (FIB) can be used to etch the lower spiral into a layer of gold film, followed by filling the slot with silicon dioxide, surface planarization and deposition of another layer of gold film. The upper spiral can then be etched with FIB. The metallic tip could be fabricated with low current electron beam-assisted local deposition [19]. Moreover, no stringent alignment between the illumination and the near-field probe is required as long as the illumination is uniform. Such a probe can be made into a two-dimensional array and the hot spots at the tip apex can be switched on and

off by modulating the polarization handedness, making this probe design very attractive for large area parallel near-field optics applications such as photolithography and imaging.

Acknowledgments

G. Rui acknowledges the support by the National Basic Research Program of China under Grant No. 2011CB301802.